Two-dimensional electron-gas actuation and transduction for GaAs nanoelectromechanical systems

H. X. Tang, X. M. H. Huang, and M. L. Roukes[a)]
Condensed Matter Physics 114-36, California Institute of Technology, Pasadena, California 91125

M. Bichler[b)] and W. Wegscheider
Institut für Experimentelle und Angewandte Physik, Universität Regensburg, D-93040 Regensburg, Germany

(Received 7 March 2002; accepted 30 August 2002)

We have fabricated doubly clamped beams from GaAs/AlGaAs quantum-well heterostructures containing a high-mobility two-dimensional electron gas (2DEG). Applying an rf drive to in-plane side gates excites the beam's mechanical resonance through a dipole–dipole mechanism. Sensitive high-frequency displacement transduction is achieved by measuring the ac emf developed across the 2DEG in the presence of a constant dc sense current. The high mobility of the incorporated 2DEG provides low-noise, low-power, and high-gain electromechanical displacement sensing through combined piezoelectric and piezoresistive mechanisms. © *2002 American Institute of Physics.*
[DOI: 10.1063/1.1516237]

Thin, suspended two-dimensional electron gas (2DEG) heterostructures have been recently perfected, and have subsequently been employed for nanoscale conducting devices.[1,2] In this letter, we present a high-resolution displacement readout that is based upon our ability to achieve very high mobility suspended quantum wires. Molecular beam epitaxial (MBE) grown materials are directly patterned and in-plane gates are used to excite the vibration. No metallization is needed, hence high Q values can be obtained.

The starting material was a specially designed, MBE-grown, 2DEG heterostructure similar to that used in Ref. 1. The structural layer stack comprises seven individual layers having a total thickness of 115 nm. The top and bottom are thin GaAs cap layers preventing oxidation of the $Al_{0.3}Ga_{0.7}As$:Si donor layers in between. The central 10-nm-thick GaAs layer forms a quantum well sustaining a high mobility 2DEG located 37 nm below the top surface and surrounded by two AlGaAs spacer layers. Below the structural layer stack is a 400 nm $Al_{0.8}Ga_{0.2}As$ sacrificial layer. The structure was intentionally made asymmetric to avoid neutralizing the piezoelectric effect of GaAs.

After ohmic contacts were deposited, a thick layer of poly-methyl-methacrylate (PMMA) is spun on the chip, followed by a single electron-beam lithography step to expose trenches in PMMA that isolate the beam from its side gates. PMMA was then employed as a direct mask against a low voltage electron cyclotron reactor etch performed to further etch the trenches to the sacrificial layer. After stripping off the PMMA, final structure relief is achieved by removing the sacrificial layer beneath the beams with diluted HF. To minimize the damage to the 2DEG from dry etching, a Cl_2/He plasma was chosen because of its excellent etching characteristics, such as smooth surface morphology and vertical sidewall. A stable etching speed at 35Å /s is obtained under conditions of less than 150 V self-bias (20 W constant rf power), Cl_2 and He flow rate ratio 1:9, 3 mTorr pressure, and 300 W microwave power. With the same method, we have also fabricated suspended Hall bars and extensively characterized the resulting suspended 2DEG. Before processing, the initial mobility and density after illumination are 5.1×10^5 cm^2/Vs, 1.26×10^{12} cm^{-2}, respectively. With our improved low damage etching, the mobility can be maintained at 2.0×10^5 cm^2/Vs, while the electron density is somewhat reduced to 4.5×10^{11} cm^{-2}. We observed well-developed quantum Hall plateaus in the etched structure even with channel width as small as 0.35 μm. In longitudinal resistance measurements, we detected a low field maximum, corresponding to maximal boundary scattering when the electron cyclotron motion diameter matches the electrical width of the suspended wire.[3] From the position of this peak, we are able to deduce the depletion to be 0.1 μm on each side of the wire. We also confirmed ballistic behavior of electrons from transport measurement on the Hall cross-junction. Both "last Hall plateau" and "negative bendresistance"[4] are present in all of the devices. The transport mean free path was found to be approximately 2 μm.

A typical device is shown in Fig. 1. The beams are 0.5 μm wide and 6 μm long, having a calculated spring constant of 0.25 N/m. When cooled to liquid helium temperature, their two-terminal resistance is about 100 kΩ. After illumination, this drops to about 5 kΩ (including contact and lead resistances). The electrical width of the beam is about 0.3 μm with $R_{\square}=170\ \Omega$.

In nanoelectromechanical system (NEMS), both the induction and the detection of motion pose important challenges. In our devices, the actuation is relatively trivial and very effective. The rf drive is supplied directly to one of the side gates, which is a large area of 2DEG connected to the output of a network analyzer through alloyed ohmic contact. All the trenches have a width of 0.5 μm. The devices are first measured at 4.2 K in vacuum. A constant dc sensing current ranging from 0 to 26 μA is supplied to the vibrating beam through a 10 mH rf choke, whose value is chosen large

[a)]Author to whom correspondence should be addressed; electronic mail: roukes@caltech.edu
[b)]Walter-Schottky-Institut der Technischen Universität München, Am Coulombwall, 85748 Garching, Germany.

 © 2002 American Institute of Physics
Downloaded 25 Feb 2006 to 131.215.240.9. Redistribution subject to AIP license or copyright, see http://apl.aip.org/apl/copyright.jsp

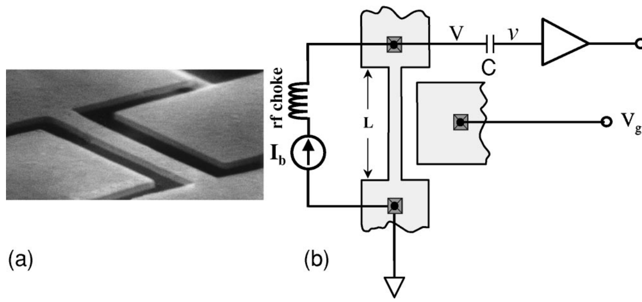

FIG. 1. (a) SEM image of a doubly clamped beam. The in-plane gates are formed by the 2DEG. (b) Sketch of measurement setup. A constant dc bias current (I_b) is sent through a large rf choke (~ 10 mH). Gate drive voltage consists of both dc and rf components: $V_g = V_g^{(0)} + v_g e^{i\omega t}$. The induced signal can be expressed as $V = V^{(0)} + v e^{I(\omega t + \varphi)}$, where the dc voltage $V^{(0)} = I_b R_{dc}$ is blocked by a capacitor C, and the oscillating component is amplified.

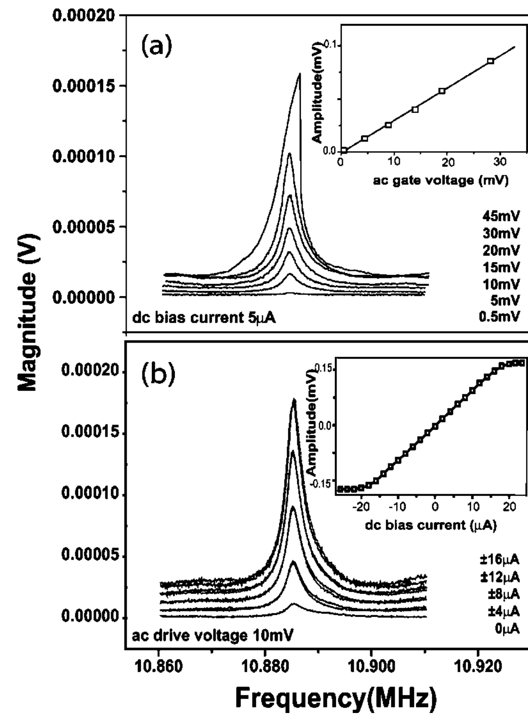

FIG. 2. Voltage drop across the beam as it is driven to its lowest mechanical resonance with increasing drive amplitudes. The dc bias current is fixed at 5 μA. Inset: The peak response as a function of driving amplitude in the linear regime. (b) Magnitude response vs dc bias current. Inset: The signal amplitude at resonance with sensing current increased from -26 to 26 μA.

enough to avoid loss of the small signal that is induced. The oscillatory signal is picked up by a low temperature amplifier placed in close proximity to the device. Before connecting the signal to the input of the network analyzer, a room temperature amplifier is used to improve signal-to-noise ratio. The combined amplifiers have a voltage gain of about 200 in the frequency range of these experiments.

We observed a very strong signal around the first mechanical resonance. The magnitude response curves at various driving amplitudes are shown in Fig. 2(a). Calculations confirm this resonance corresponds to the first out-of-plane vibrational mode. When the drive amplitude is increased above 45 mV, the response curve becomes nonlinear and assumes an asymmetric shape. In the linear response region, the amplitude at resonance is proportional to the ac gate voltage amplitude.

To clarify the origin of the observed signal, we fixed the drive at 10 mV and then varied the dc bias current from -26 μA to 0 and then to 26 μA. The response amplitude versus drive amplitude at resonance is presented in Fig. 2(b). Two features are evident from this data. First, at the highest currents close to 20 μA, the signal becomes saturated for two reasons: (a) Joule heating of the small beam, and (b), saturation of the drift velocity at high applied electrical fields (~ 15 kV/m). Second, at intermediate current the signal strength at resonance is proportional to the dc bias current, as indicated in the inset of Fig. 2(b). In addition, when we reverse the current direction, we also find that the induced signal changes its sign (180° phase change). Therefore, we conclude that the dominant contribution to the observed signal is a change of resistance due to beam vibration. This appears to originate from both piezoresistive effect of bulk GaAs and transverse piezoelectric charge gating of 2DEG. Note that a small signal is observed even for zero current bias. From the slope of the linear part in the inset of Fig. 2(b), a nominal drive of 10 mV induces a resistance change of about 10 Ω in the device.

We now estimate the sensitivity of this technique. By looking at the critical amplitude at the onset of nonlinearity, we can determine the amplitude of vibration of the resonating beam. This critical displacement amplitude depends only on the geometry of the beam, and is approximately given as[5] $x_c \sim (2h)/\sqrt{0.5Q(1-\nu^2)}$, where h is the thickness of the beam in the vibration direction, and ν is Poisson's ratio for GaAs. Plugging in measured values of $Q = 2600$ and $\nu = 0.31$, we obtain $x_c = 6$ nm, which is attained at a drive level of about 45 mV. The minimum resolvable signal is achieved at 0.1 mV drive and about 5 μA sensing current. Hence, at the highest possible current of 20 μA, we can detect a resonance at $x_c/450/4 = 0.03$ Å, or 3×10^{-3} Å/$\sqrt{\text{Hz}}$, which is consistent with our estimate based on Johnson noise from beam resistance at 4.2 K. The corresponding force sensitivity is 75 fN/$\sqrt{\text{Hz}}$, comparable with previous schemes to detect small NEMS resonators by optical interferometry[6] and the magnetomotive method.[7] The required force to drive the beam to the nonlinearity threshold is 1.5 nN. The displacement resolution can be improved by using 2DEG heterostructures with even higher mobility, or by operating at ~ 100 mK with a state-of-the-art low temperature preamplifier.

Note that in Fig. 2, all the driving force results from the applied ac gate voltage. We did not find any significant change of resonant frequency or magnitude with dc bias on the gate. This is indicative of a coupling mechanism different from electrostatic force between the gates and the beam. Electrostatic force is proportional to the product of dc and ac components of gate potential so that the response should directly scale with the dc gate voltage.[8] This assumes a direct Coulomb interaction between coupling plates. In our in-plane-gate configuration, the net charge on the beam is $C(V_g^{(0)} + v_g e^{i\omega t})$. The capacitance between coplanar 2DEG areas has an estimated value of 18 aF/μm,[9] which is very small compared to parallel plates. With a nominal 1 V dc gate voltage, there are only a few hundred induced electron charges on the beam. The upper bound of the electric field

Downloaded 25 Feb 2006 to 131.215.240.9. Redistribution subject to AIP license or copyright, see http://apl.aip.org/apl/copyright.jsp

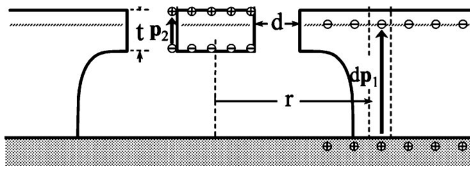

FIG. 3. A cross-sectional schematic of the dipolar actuation mechanism, showing dipole formation on the beam (p_1) and on the driving gate (dp_2).

applied on the gate is $(V_g^{(0)}+v_g e^{i\omega t})/d$, d is the beam–gate separation (Fig. 3). Thus, the total electrostatic force applied on the beam with angular frequency ω is $f = CV_g^{(0)} v_g e^{i\omega t}/d$. Only a projection of this force drives the beam along the out-of-plane (y) direction. A reasonable estimate of the effective y-component of this force is

$$f_y = CV_g^{(0)} v_g e^{i\omega t} y_0/d^2, \tag{1}$$

where y_0 is a static offset due to, for example, uncontrolled asymmetry of suspended beam. A 10 nm misalignment of the beam with respect to gate should be observable in our devices (but is not seen). Therefore, we take this number as the upper limit in our estimation of y_0. At a nominal 1 V dc gate voltage, 45 mV ac gate voltage, the force originating from the electrostatic drive mechanism is calculated to be $f_y \approx 0.2$ pN. This is four orders of magnitude smaller than the force required to drive the beam into nonlinear response.

Given the absence of direct electrostatic forces, we propose a new driving mechanism, a short–range dipole-dipole interaction. This dipole–dipole interaction potential can be expressed as $U = \int (1/4\pi\varepsilon_0)\ (p_2 dp_1/r^3)$, which can be understood as rf coupling between two dipole moments dp_1 and p_2. Here dp_1 is the dipole momentum of a slice of the gate, $dp_1 = \varepsilon_r \varepsilon_0 L v_g e^{i\omega t} dr$, and p_2 is the fixed dipole moment due to the piezoelectric effect within the strained beam. y is the beam displacement, $p_2 = 3Ed_A wt^2 y/L$, and L, w, and t are beam length, width and thickness, respectively (Fig. 3). ε_r is dielectric constant of GaAs. Here, $E \sim 85$ Gpa is Young's modulus and $d_A \sim 3.8$ pC/N is the piezoelectric constant of AlGaAs.[10] The resulting force along y direction is

$$f_y = \frac{\partial U}{\partial y} = \frac{3\varepsilon_r}{4\pi}(Ed_A)\left(\frac{wt^2}{d^2}\right) v_g e^{i\omega t}. \tag{2}$$

This dynamic force is *independent* of the dc gate voltage, consistent with our observation. After structural relief, the suspended beams are intrinsically stressed due to the heterostructure's asymmetry and other factors. Therefore, a static dipole moment exists on the beam and yields the out-of-plane vibration. At 45 mV ac gate voltage drive, f_y is estimated to be 1.2 nN from this mechanism, four orders of magnitude higher than the direct Coulomb interaction. This is consistent with the force we observe at the onset of nonlinearity. Because of its short-range characteristics, this dipole–dipole interaction is unique to NEMS and is insignificant in microelectromechanical systems.

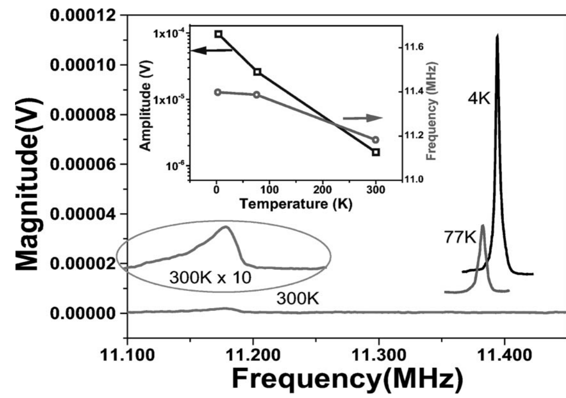

FIG. 4. (a) SEM image of a doubly clamped beam. The in-plane gates are formed by the 2DEG. (b) Sketch of measurement setup. A constant dc bias current (I_b) is sent through a large rf choke ($\sim$10 mH) before reaching the beam. Gate drive voltage consists of both dc and rf components: $V_g = V_g^{(0)} + v_g e^{i\omega t}$. The induced signal can be expressed as $V = V^{(0)} + ve^{i(\omega t+\varphi)}$, where the dc voltage potential $V^{(0)} = I_b R_{dc}$ is blocked by a capacitor C, and the oscillating component is amplified at both liquid helium and room temperature.

We have also studied the temperature dependence of our strain sensitive devices. Measurements were performed at three different temperatures in vacuum. The results are shown in Fig. 4. The devices perform exceptionally well at liquid helium and nitrogen temperatures, but at room temperature, the response is diminished. The decay of signal strength with temperature can be attributed to the significant reduction of 2DEG mobility. At elevated temperature the increased two-terminal beam resistance acts as a large voltage divider, and only a small fraction of induced signal voltage is available.

We gratefully acknowledge support from DARPA, through Grant No. DABT63-98-1-0012, and the NSF via grant ECS-0089061. We also thank F. G. Monzon and J. Casey for early contributions to this work, and J. Y. T. Yang and K. Cooper for help with the low temperature amplifier.

[1] R. H. Blick, F. G. Monzon, W. Wegscheider, M. Bichler, F. Stern, and M. L. Roukes, Phys. Rev. B **62**, 17103 (2000).
[2] R. G. Beck, M. A. Eriksson, R. M. Westervelt, K. L. Campman, and A. C. Gossard, Appl. Phys. Lett. **68**, 3763 (1996); R. G. Beck, R. G. Eriksson, M. A. Topinka, R. M. Westervelt, K. D. Maranowski, and A. C. Gossard, Appl. Phys. Lett. **73**, 1149 (1998).
[3] T. J. Thornton, M. L. Roukes, A. Scherer, and B. P. Van de Gaag, Phys. Rev. Lett. **63**, 2128 (1989).
[4] M. L. Roukes, A. Scherer, S. J. Allen, H. G. Craighead, R. M. Ruthen, E. D. Reebe, and J. P. Harbison, Phys. Rev. Lett. **59**, 3011 (1987).
[5] H. A. C. Tilmans, M. Elwenspoek, and J. H. J. Fluitman, Sens. Actuators A **30**, 35 (1992).
[6] D. W. Carr, S. Evoy, L. Sekaric, H. G. Craighead, and J. M. Parpia, Appl. Phys. Lett. **75**, 920 (1999).
[7] A. N. Cleland and M. L. Roukes, Appl. Phys. Lett. **75**, 920 (1996).
[8] D. Rugar and P. Grütter, Phys. Rev. Lett. **67**, 699 (1991).
[9] D. K. de Vries, P. Stelmaszyk, and A. D. Wieck, J. Appl. Phys. **79**, 8087 (1996).
[10] K. Fricke, J. Appl. Phys. **70**, 914 (1991).

Downloaded 25 Feb 2006 to 131.215.240.9. Redistribution subject to AIP license or copyright, see http://apl.aip.org/apl/copyright.jsp